ISSN 1674-1056
http://cpb.iphy.ac.cn
http://iopscience.iop.org/cpb
中国物理 B
Chinese Physics
中国物理
Chinese Physics B

Coupling between velocity and interface perturbations in cylindrical Rayleigh-Taylor instability

Hong-Yu Guo(郭宏宇), Li-Feng Wang(王立锋), Wen-Hua Ye(叶文华), Jun-Feng Wu(吴俊峰), Wei-Yan Zhang(张维岩)

Citation: Chin. Phys. B . 2018, 27(5): 055205. **doi:** 10.1088/1674-1056/27/5/055205

Journal homepage: http://cpb.iphy.ac.cn; http://iopscience.iop.org/cpb

What follows is a list of articles you may be interested in

Rayleigh-Taylor instability at spherical interfaces of incompressible fluids

Hong-Yu Guo(郭宏宇), Li-Feng Wang(王立锋), Wen-Hua Ye(叶文华), Jun-Feng Wu(吴俊峰), Ying-Jun Li(李英骏), Wei-Yan Zhang(张维岩)
Chin. Phys. B . 2018, 27(2): 025206. **doi:** 10.1088/1674-1056/27/2/025206

Rayleigh-Taylor instability of multi-fluid layers in cylindrical geometry

Hong-Yu Guo(郭宏宇), Li-Feng Wang(王立锋), Wen-Hua Ye(叶文华), Jun-Feng Wu(吴俊峰), Wei-Yan Zhang(张维岩)
Chin. Phys. B . 2017, 26(12): 125202. **doi:** 10.1088/1674-1056/26/12/125202

Magneto-Rayleigh–Taylor instability in compressible Z-pinch liner plasmas

Xue Yang(杨学), De-Long Xiao(肖德龙), Ning Ding(丁宁), Jie Liu(刘杰)
Chin. Phys. B . 2017, 26(7): 075202. **doi:** 10.1088/1674-1056/26/7/075202

Cylindrical effects in weakly nonlinear Rayleigh–Taylor instability

Liu Wan-Hai, Ma Wen-Fang, Wang Xu-Lin
Chin. Phys. B . 2015, 24(1): 015202. **doi:** 10.1088/1674-1056/24/1/015202

Diagnostic technique for measuring fusion reaction rate for inertial confinement fusion experiments at Shen Guang-III prototype laser facility

Wang Feng, Peng Xiao-Shi, Kang Dong-Guo, Liu Shen-Ye, Xu Tao
Chin. Phys. B . 2013, 22(11): 115204. **doi:** 10.1088/1674-1056/22/11/115204

Coupling between velocity and interface perturbations in cylindrical Rayleigh–Taylor instability*

Hong-Yu Guo(郭宏宇)[1,2], Li-Feng Wang(王立锋)[2,3], Wen-Hua Ye(叶文华)[2,3,†], Jun-Feng Wu(吴俊峰)[2], and Wei-Yan Zhang(张维岩)[2,3]

[1] *Graduate School, China Academy of Engineering Physics, Beijing* 100088, *China*
[2] *Institute of Applied Physics and Computational Mathematics, Beijing* 100094, *China*
[3] *HEDPS, Center for Applied Physics and Technology, Peking University, Beijing* 100871, *China*

(Received 9 September 2017; revised manuscript received 11 January 2018; published online 26 April 2018)

Rayleigh–Taylor instability (RTI) in cylindrical geometry initiated by velocity and interface perturbations is investigated analytically through a third-order weakly nonlinear (WN) model. When the initial velocity perturbation is comparable to the interface perturbation, the coupling between them plays a significant role. The difference between the RTI growth initiated only by a velocity perturbation and that only by an interface perturbation in the WN stage is negligibly small. The effects of the mode number on the first three harmonics are discussed respectively. The low-mode number perturbation leads to large amplitudes of RTI growth. The Atwood number and initial perturbation dependencies of the nonlinear saturation amplitude of the fundamental mode are analyzed clearly. When the mode number of the perturbation is large enough, the WN results in planar geometry are recovered.

Keywords: Rayleigh–Taylor instability, weakly nonlinear, cylindrical geometry

PACS: 52.57.Fg, 47.20.Ma, 52.35.Py **DOI:** 10.1088/1674-1056/27/5/055205

1. Introduction

When a heavier fluid is accelerated by a lighter one or supported by a lighter fluid in a gravitational field, a perturbed interface between the two fluids is subject to the Rayleigh–Taylor instability (RTI).[1,2] The RTI plays a critical role in many areas such as *Z*-pinch[3] and inertial confinement fusion (ICF).[4,5] In typical ICF implosions, a spherical capsule containing an ablator-fuel shell filled with deuterium–tritium gas is imploded inward by lasers or x-rays. The major problem plaguing high-compression ICF implosions is the RTI.[6] In the acceleration stage, the outer interface of the shell is the RTI. In the deceleration stage, the inner interface of the imploded shell is subject to the RTI. The evolution of the RTI growth leads to the mixing of the ablator material into the hot-spot. The RTI growth can also cause deformation of the hot-spot and even break up the shell, resulting in ignition failure. Thus, RTI growth must be limited to an acceptable level. The RTI still remains an important issue that needs to be carefully investigated in the ICF community.

The classical RTI was first studied by Rayleigh,[1] where a semi-infinite fluid of density ρ_a is accelerated by another semi-infinite fluid of density ρ_b ($\rho_a > \rho_b$). A small amplitude perturbation with wave number k on the interface between the two fluids will grow exponentially, $\eta(t) \sim \eta_0 e^{\gamma t}$, where η_0 is the initial small amplitude of the perturbation. The $\gamma = \sqrt{Akg}$ is the linear growth rate of the RTI perturbation with g being the acceleration. The $A = (\rho_a - \rho_b)/(\rho_a + \rho_b)$ is the Atwood number at the interface. Based on this classical model, the RTI has been extensively explored analytically,[7–11] numerically [12–14] and experimentally.[6] Mikaelian[9] extended the classical RTI to the multi-fluid RTI. The linear growth rate of the multi-fluid RTI was discussed in his linear model. The magnetic field width effect dramatically reduces the linear growth rate of the RTI, which was discussed by Yang.[11] When the amplitude of the perturbation is comparable to the perturbation wave length, the nonlinear mode-coupling effect becomes pronounced. Before a strong nonlinear stage, there exists a weakly nonlinear (WN) phase. The WN growth of RTI has been studied extensively.[15–22] Three-dimensional RTI growth in the WN phase was analytically studied by Jacobs[15] for initially varied perturbation symmetries. Reference [16] investigated the third-order WN growth of RTI for an arbitrary Atwood number considering the effect of surface tension. The multi-mode perturbation of RTI was discussed by Haan[17] through the second-order solution. Garnier[18] explored a WN model for the ablative RTI. It was found that the WN growth of ablative RTI is clearly reduced in comparison to the classical RTI. The WN model of RTI for a finite-thickness fluid slab was developed in Ref. [19], where the feedthrough effect of a thin shell was analyzed. All the models mentioned above are restricted to planar systems. However, the RTI always occurs in non-Cartesian coordinate systems, such as ICF implosions and magnetized liner inertial fusion (MagLIF) experiments.[23] In

*Project supported by the National Natural Science Foundation of China (Grant Nos. 11275031, 11475034, 11575033, and 11274026) and the National Basic Research Program of China (Grant No. 2013CB834100).

†Corresponding author. E-mail: ye_wenhua@iapcm.ac.cn

© 2018 Chinese Physical Society and IOP Publishing Ltd

real ICF implosions, the final implosion capsule performance is mainly determined by the perturbation seeds early in the implosion. The perturbation sources are generally from the driver aspect and the implosion capsule. The interface perturbation of the capsule part is primarily from the shell surface roughness or the surface imperfection. During the implosion, the deceleration phase starts after the return shock reflects off the center of the implosion target and interacts with the inner surface of the imploded shell. When the shell interacts with the return shock, the shell is slowed down in an impulsive pattern. The inner interface is subject to the Richtmyer–Meshkov instability (RMI)[24,25] because of the impulsive deceleration (typically twice). Furthermore, this RMI can further influence the phase and the amplitude of the subsequent RTI growth due to the fact that the RMI acts as a seed for the following RTI growth.[5,26] This means the initial perturbation of the RTI in ICF implosions has not only interface perturbations but also velocity perturbations. The RTI growth in cylindrical geometry initiated with velocity perturbation has been studied by Wang.[27] In this paper, the coupled WN solutions of the cylindrical RTI initiated by both velocity and interface perturbations are analyzed.

This paper is organized as follows. Section 2 describes the theoretical model of the RTI growth. The WN growth of the cylindrical RTI is discussed in Section 3. Section 4 summarizes the major results and gives some conclusions.

2. Theoretical model

In this section, we will provide the governing equations of the system. The WN solutions of the perturbation growth are also derived. The cylindrical coordinate system is established in the present work, where r and θ are along and normal to the undisturbed fluid interface, respectively. We consider two incompressible, irrotational, inviscid and immiscible fluids separated by a cylindrical interface, which are immersed in a gravitational field $\boldsymbol{g} = -g\boldsymbol{e}_r$ (i.e., the hot-spot interface during the deceleration stage of the ICF implosion). The perturbed fluid interface can be expressed as $r(t,\theta) = R + \eta(t,\theta)$, where R is radius of the initially unperturbed interface and $\eta(t,\theta)$ is the small perturbation. In the following discussion, the physical quantities of the interior fluid ($0 < r < R$) shall be denoted by the superscript "i" and those of the exterior fluid ($R < r < \infty$) by "e". The governing equations for the present system are

$$\nabla^2\phi^{\mathrm{i}} = \nabla^2\phi^{\mathrm{e}} = 0, \tag{1}$$

$$\begin{aligned}&\frac{\partial\eta}{\partial t} + \frac{1}{r^2}\frac{\partial\eta}{\partial\theta}\frac{\partial\phi^{\mathrm{i}}}{\partial\theta} - \frac{\partial\phi^{\mathrm{i}}}{\partial r}\\ =\ &\frac{\partial\eta}{\partial t} + \frac{1}{r^2}\frac{\partial\eta}{\partial\theta}\frac{\partial\phi^{\mathrm{e}}}{\partial\theta} - \frac{\partial\phi^{\mathrm{e}}}{\partial r} = 0 \ \text{ at } \ r = R+\eta,\end{aligned} \tag{2}$$

$$\begin{aligned}&\rho^{\mathrm{i}}\left\{\frac{\partial\phi^{\mathrm{i}}}{\partial t} + \frac{1}{2}\left(\frac{\partial\phi^{\mathrm{i}}}{\partial r}\right)^2 + \frac{1}{2r^2}\left(\frac{\partial\phi^{\mathrm{i}}}{\partial\theta}\right)^2 + gr\right\}\\ &-\rho^{\mathrm{e}}\left\{\frac{\partial\phi^{\mathrm{e}}}{\partial t} + \frac{1}{2}\left(\frac{\partial\phi^{\mathrm{e}}}{\partial r}\right)^2 + \frac{1}{2r^2}\left(\frac{\partial\phi^{\mathrm{e}}}{\partial\theta}\right)^2 + gr\right\} = f(t)\\ &\text{at } \ r = R+\eta,\end{aligned} \tag{3}$$

where ρ^{i} and ρ^{e} are densities ($\rho^{\mathrm{e}} > \rho^{\mathrm{i}}$). ϕ^{i} and ϕ^{e} are the perturbed velocity potentials relating to the fluid velocities, and $f(t)$ is an arbitrary function of time. The two incompressible fluids are described by the Laplace equation (1). According to the kinematic boundary conditions of Eq. (2), the normal velocity of each fluid across the interface is continuous. Equation (3) represents the continuous condition of the pressure across the interface.

Considering a small-amplitude cosinusoidal perturbation, the amplitude of the perturbation $\eta(t,\theta)$ and the perturbed velocity potentials $\phi^{\mathrm{i}}(t,r,\theta)$ and $\phi^{\mathrm{e}}(t,r,\theta)$ can be expanded into a power series in a formal parameter ϵ

$$\begin{aligned}&\eta(t,\theta)\\ =\ &\epsilon\eta_{1,1}(t)\cos(m\theta) + \epsilon^2\eta_{2,0}(t) + \epsilon^2\eta_{2,2}(t)\cos(2m\theta)\\ &+\epsilon^3\eta_{3,1}(t)\cos(m\theta) + \epsilon^3\eta_{3,3}(t)\cos(3m\theta) + O(\epsilon^4),\end{aligned} \tag{4}$$

$$\begin{aligned}&\phi^{\mathrm{i}}(t,r,\theta)\\ =\ &\epsilon c_{1,1}(t)r^m\cos(m\theta) + \epsilon^2 c_{2,0}(t)\\ &+\epsilon^2 c_{2,2}(t)r^{2m}\cos(2m\theta) + \epsilon^3 c_{3,1}(t)r^m\cos(m\theta)\\ &+\epsilon^3 c_{3,3}(t)r^{3m}\cos(3m\theta) + O(\epsilon^4),\end{aligned} \tag{5}$$

$$\begin{aligned}&\phi^{\mathrm{e}}(t,r,\theta)\\ =\ &\epsilon d_{1,1}(t)r^{-m}\cos(m\theta) + \epsilon^2 d_{2,0}(t)\\ &+\epsilon^2 d_{2,2}(t)r^{-2m}\cos(2m\theta) + \epsilon^3 d_{3,1}(t)r^{-m}\cos(m\theta)\\ &+\epsilon^3 d_{3,3}(t)r^{-3m}\cos(3m\theta) + O(\epsilon^4),\end{aligned} \tag{6}$$

where m is the mode number of the perturbation. $\eta_{p,p-2q}(t)$ $[c_{p,p-2q}(t), d_{p,p-2q}(t)]$ is the amplitude of the $(p-2q)$-th-order Fourier harmonic of the perturbation (the velocity potential) in the p-th order of ϵ. Here, $p = 1,2,3$ and $q = 0,\ldots,\lfloor p/2\rfloor$, the Gauss symbol $\lfloor p/2\rfloor$ means a maximum integer less than or equal to $p/2$. It should be noted that the velocity potentials $\phi^{\mathrm{i}}(t,r,\theta)$ and $\phi^{\mathrm{e}}(t,r,\theta)$ have satisfied the Laplace equation (1). The amplitudes of the perturbation $\eta_{p,p-2q}(t)$ at the interface are the unknowns that we want to obtain.

First, we substitute Eqs. (4)–(6) into the governing equations (2) and (3). Then, we take a series expansion for the governing equations at the perturbed interface $R+\eta$. Based on the Taylor series theory, the boundary conditions are expanded at the interface with the expansion parameter ϵ. Collecting the terms with the same order of ϵ yields the p-th-order equations containing ϵ^p. Lastly, the amplitudes of the p-th-order Fourier harmonic are derived by successively solving the obtained p-th-order equations, which will be discussed below.

In a real system (i.e., ICF implosion), when the RTI starts to grow, there will be both interface and velocity perturbations on the interface.[5] Here, we consider an initially single-mode

cosinusoidal perturbation, namely, $\eta(t=0,\theta)=\alpha\cos(m\theta)$ and $v_0(t=0,\theta)=v\gamma\cos(m\theta)$. This most common initial condition can be rewritten as

$$\eta_{p,p-2q}\big|_{t=0}=\alpha\delta_{1p}, \tag{7}$$

$$\dot{\eta}_{p,p-2q}\big|_{t=0}=v\gamma\delta_{1p}, \tag{8}$$

where α and v are the perturbation amplitudes, $\gamma=\sqrt{Amg/R}$ is the linear growth rate in the cylindrical geometry.[5] $A=(\rho^{\rm e}-\rho^{\rm i})/(\rho^{\rm e}+\rho^{\rm i})$ is the Atwood number. δ_{1p} is the Kronecker delta function with $p=1,2,3$. The overdot represents the time derivative.

At the first-order $O(\epsilon)$, the ordinary differential equation (ODE) for the linear growth is

$$\ddot{\eta}_{1,1}-\gamma^2\eta_{1,1}=0, \tag{9}$$

which is a well-known equation[5,21] for the fundamental generation. The overdot represents the time derivative. Using the initial condition $\eta_{1,1}(0)=\alpha$ and $\dot{\eta}_{1,1}(0)=v\gamma$, we obtain

$$\eta_{1,1}=\overbrace{\alpha\cosh(\Gamma)+v\sinh(\Gamma)}^{(\boldsymbol{k})}, \tag{10}$$

which describes the linear growth of RTI in the cylindrical geometry, which is quite similar to the result in the planar case. The $\Gamma=\gamma t$ is the normalized growth rate.

At the second-order $O(\epsilon^2)$, the ODE for $\eta_{2,2}$ is

$$\ddot{\eta}_{2,2}-2\gamma^2\eta_{2,2}+A\frac{m}{R}\dot{\eta}_{1,1}^2+\frac{1}{2R}\left(\dot{\eta}_{1,1}^2+\eta_{1,1}\ddot{\eta}_{1,1}\right)=0, \tag{11}$$

which is a second-order ODE with constant coefficient. By adopting the initial conditions $\eta_{2,2}(0)=0$ and $\dot{\eta}_{2,2}(0)=0$, we have

$$\begin{aligned}\eta_{2,2}=-\frac{1}{4R}\Bigg\{&\left[\alpha^2+v^2(2Am+1)\right]\overbrace{\sinh^2(\Gamma)}^{(\boldsymbol{k},\boldsymbol{k})}\\&+\left[v^2+\alpha^2(2Am+1)\right]\left[\overbrace{\cosh^2(\Gamma)}^{(\boldsymbol{k},\boldsymbol{k})}-\overbrace{\cosh(\sqrt{2}\Gamma)}^{(2\boldsymbol{k})}\right]\\&+2\alpha v(Am+1)\left[2\overbrace{\cosh(\Gamma)\sinh(\Gamma)}^{(\boldsymbol{k},\boldsymbol{k})}-\sqrt{2}\overbrace{\sinh(\sqrt{2}\Gamma)}^{(2\boldsymbol{k})}\right]\Bigg\}.\end{aligned} \tag{12}$$

As can be seen in Eq. (12), there is a coupling term, i.e., term αv, between the velocity and interface perturbations. The second harmonic feedback to the zero harmonic equation takes the form

$$\dot{\eta}_{2,0}+\frac{1}{2R}\eta_{1,1}\dot{\eta}_{1,1}=0, \tag{13}$$

with the initial condition $\eta_{2,0}(0)=0$, the solution of the second-order feedback to the zero harmonic can be written as

$$\eta_{2,0}=-\frac{1}{4R}\left(\alpha^2+v^2\right)\overbrace{\sinh^2(\Gamma)}^{(\boldsymbol{k},-\boldsymbol{k})}-\frac{1}{2R}\alpha v\overbrace{\cosh(\Gamma)\sinh(\Gamma)}^{(\boldsymbol{k},-\boldsymbol{k})}, \tag{14}$$

the $\eta_{2,0}$ is generated from the mode-coupling of the fundamental mode, which vanishes in the planar geometry.

At the third-order $O(\epsilon^3)$, the second-order ODE for $\eta_{3,3}$ is

$$\begin{aligned}&\ddot{\eta}_{3,3}-3\gamma^2\eta_{3,3}+\frac{3m^2}{4R^2}\dot{\eta}_{1,1}^2\eta_{1,1}+3A\frac{m}{R}\dot{\eta}_{1,1}\dot{\eta}_{2,2}\\&+\frac{1}{2R}\left(2\dot{\eta}_{1,1}\dot{\eta}_{2,2}+\eta_{2,2}\ddot{\eta}_{1,1}+\eta_{1,1}\ddot{\eta}_{2,2}\right)=0,\end{aligned} \tag{15}$$

and the third-order feedback to the fundamental mode is

$$\begin{aligned}&\ddot{\eta}_{3,1}-\gamma^2\eta_{3,1}+\frac{m^2}{4R^2}(\eta_{1,1}\dot{\eta}_{1,1}^2+\eta_{1,1}^2\ddot{\eta}_{1,1})\\&+A\frac{m}{R}(\dot{\eta}_{1,1}\dot{\eta}_{2,0}-\eta_{2,2}\ddot{\eta}_{1,1}-\dot{\eta}_{1,1}\dot{\eta}_{2,2})\\&+\frac{1}{2R}(\eta_{2,2}\ddot{\eta}_{1,1}+\eta_{1,1}\ddot{\eta}_{2,2}+2\dot{\eta}_{1,1}\dot{\eta}_{2,2}+2\eta_{2,0}\ddot{\eta}_{1,1}+2\dot{\eta}_{1,1}\dot{\eta}_{2,0})\\&+\frac{1}{4R^2}(Am-2)(\eta_{1,1}^2\ddot{\eta}_{1,1}+2\eta_{1,1}\dot{\eta}_{1,1}^2)=0.\end{aligned} \tag{16}$$

By applying conditions $\eta_{3,3}(0)=0$, $\dot{\eta}_{3,3}(0)=0$, $\eta_{3,1}(0)=0$ and $\dot{\eta}_{3,1}(0)=0$, the third-order solutions can be expressed as

$$\begin{aligned}\eta_{3,3}=\frac{1}{32R^2}\Bigg\{&\overbrace{a_1\cosh(\Gamma)^3+a_2\sinh(\Gamma)^3}^{(\boldsymbol{k},\boldsymbol{k},\boldsymbol{k})}+a_3\overbrace{\cosh(\Gamma)^2\sinh(\Gamma)}^{(\boldsymbol{k},\boldsymbol{k},\boldsymbol{k})}+a_4\overbrace{\sinh(\Gamma)^2\cosh(\Gamma)}^{(\boldsymbol{k},\boldsymbol{k},\boldsymbol{k})}\\&-a_5\overbrace{\cosh(\sqrt{2}\Gamma)\cosh(\Gamma)}^{(2\boldsymbol{k},\boldsymbol{k})}-a_6\overbrace{\cosh(\sqrt{2}\Gamma)\sinh(\Gamma)}^{(2\boldsymbol{k},\boldsymbol{k})}-a_7\overbrace{\sinh(\sqrt{2}\Gamma)\cosh(\Gamma)}^{(2\boldsymbol{k},\boldsymbol{k})}\\&-a_8\overbrace{\sinh(\sqrt{2}\Gamma)\sinh(\Gamma)}^{(2\boldsymbol{k},\boldsymbol{k})}+\overbrace{a_9\cosh(\sqrt{3}\Gamma)+a_{10}\sinh(\sqrt{3}\Gamma)}^{(3\boldsymbol{k})}\Bigg\},\end{aligned} \tag{17}$$

$$\eta_{3,1}=-\frac{1}{16R^2}\Bigg\{\overbrace{b_1\cosh(\Gamma)^3+b_2\sinh(\Gamma)^3}^{(\boldsymbol{k},\boldsymbol{k},-\boldsymbol{k})}+b_3\overbrace{\cosh(\Gamma)^2\sinh(\Gamma)}^{(\boldsymbol{k},\boldsymbol{k},-\boldsymbol{k})}-b_4\overbrace{\sinh(\Gamma)^2\cosh(\Gamma)}^{(\boldsymbol{k},\boldsymbol{k},-\boldsymbol{k})}$$

$$-b_1\overbrace{\cosh(\sqrt{2}\Gamma)\cosh(\Gamma)}^{(2\boldsymbol{k},-\boldsymbol{k})}-b_5\overbrace{\cosh(\sqrt{2}\Gamma)\sinh(\Gamma)}^{(2\boldsymbol{k},-\boldsymbol{k})}+b_6\overbrace{\sinh(\sqrt{2}\Gamma)\cosh(\Gamma)}^{(2\boldsymbol{k},-\boldsymbol{k})}$$
$$+b_7\overbrace{\sinh(\sqrt{2}\Gamma)\sinh(\Gamma)}^{(2\boldsymbol{k},-\boldsymbol{k})}-\overbrace{b_8\Gamma\cosh(\Gamma)-b_9\Gamma\sinh(\Gamma)}^{(\boldsymbol{k},-\boldsymbol{k},\boldsymbol{k})}\Big\}, \tag{18}$$

where the coefficients $a_1,\ldots,a_{10}$ and $b_1,\ldots,b_9$ are functions of A, m, α, and v, which are explicitly shown in the Appendix. The mode-coupling property is displayed clearly in Eqs. (17) and (18). In the third-order solutions, the coupling terms containing $\alpha^2 v$ and αv^2 are generated. It should be noted that the WN results in planar geometry[20,21] are recovered for short-wavelength perturbation (high mode number m) compared to the interface radius R, namely, $\lambda = 2\pi R/m \ll R$. This means that the behavior of high mode number perturbation in cylindrical geometry is quite similar to that in planar geometry. Thus, the cylindrical convergence effect plays a critical role for low mode perturbations, which will be discussed later. The explicit initial amplitudes α and v dependencies of the RTI growth are exhibited in the following.

3. Results and discussion

In this section, the cylindrical interface positions initiated by the velocity and interface perturbations, respectively, are analyzed. The temporal evolutions of the first three harmonics are discussed. Based on the third-order WN solutions, the nonlinear saturation amplitude (NSA) of the RTI growth is also investigated.

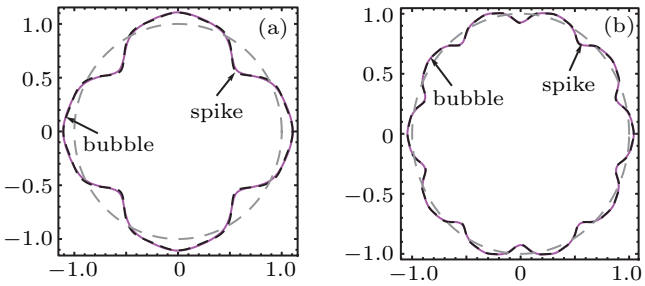


Fig. 1. (color online) Temporal evolution of the perturbed interface positions for mode number (a) $m = 4$ and (b) $m = 10$ at normalized time $\Gamma = 3.8$. The RTI growth is initiated by only the interface perturbation $\alpha = 0.004\lambda$ (solid lines) or only the velocity perturbation $v = 0.004\lambda$ (dashed lines), for Atwood number $A = 1$.

In Fig. 1, the WN evolutions of the interface position initiated by velocity perturbation alone and interface perturbation alone are plotted for $m = 4$ and 10. As can be seen obviously in Fig. 1, the initially cosinusoidal interface becomes considerable outside-to-inside asymmetric for $\Gamma = 3.8$. This bubble-spike structure can be seen clearly, especially for the low-mode number perturbation. One can also see that the cylindrical interface initiated by a velocity perturbation alone is almost identical to the case by an interface perturbation alone for $m = 10$. The difference at the spike is negligibly small between the RTI growth initiated by only the interface perturbation and that by only the velocity perturbation for $m = 4$. This means that the WN growth of cylindrical RTI initiated by an interface perturbation can be asymptotically obtained by imposing an equivalent velocity perturbation.

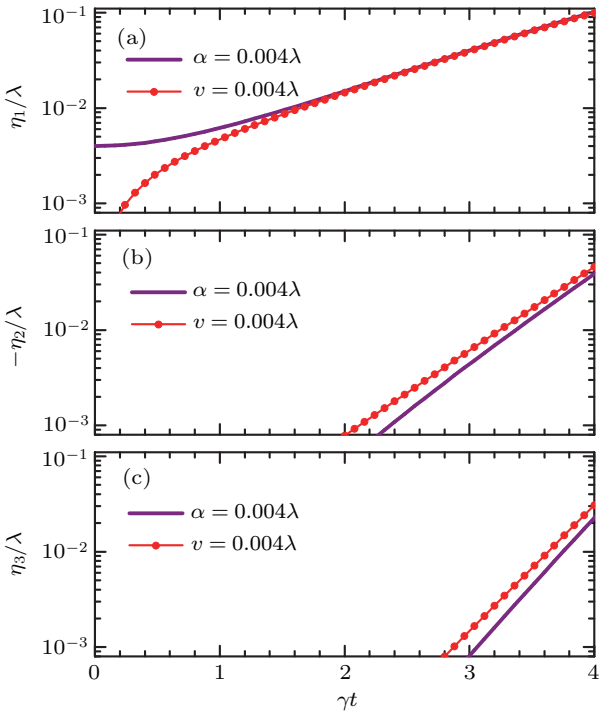


Fig. 2. (color online) Temporal evolutions of normalized amplitude of (a) the fundamental mode η_1/λ, (b) the second harmonic $-\eta_2/\lambda$, and (c) the third harmonic η_3/λ for $m = 4$ at $A = 1$. The solid lines represent the results initiated only by an interface perturbation with $\alpha = 0.004\lambda$, the dashed lines are initiated only by a velocity perturbation with $v = 0.004\lambda$.

The temporal evolutions of the normalized first three harmonics are illustrated in Fig. 2, where the perturbation growth is initiated with, respectively, a velocity perturbation and an interface perturbation. The normalized amplitude η_1/λ from the interface perturbation alone is larger than that from the velocity perturbation alone for $\gamma t < 2$. With time proceeding, the fundamental modes tend to grow equally. However, the normalized second harmonic η_2/λ and third harmonic η_3/λ initiated by velocity perturbations alone are larger than that by interface perturbations alone at fixed γt. The larger the second harmonic is, the narrower and the larger the spikes will be,[20] this phenomenon can also be seen in Fig. 1(a).

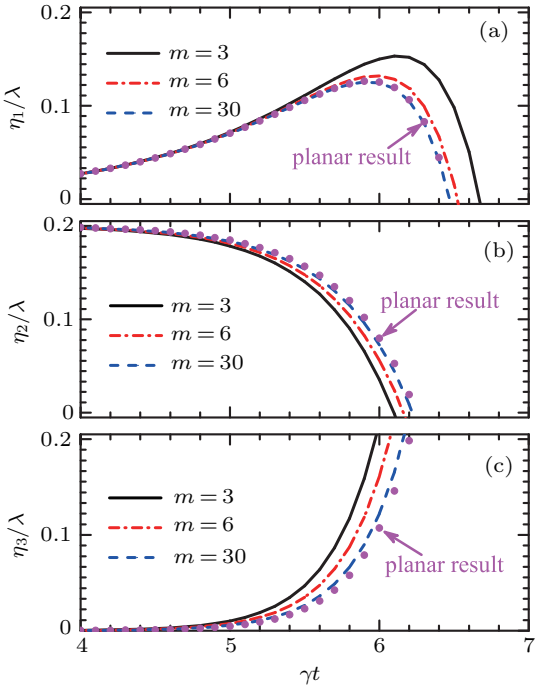


Fig. 3. (color online) The evolutions of the normalized amplitudes of (a) the fundamental mode η_1/λ, (b) the second harmonic η_2/λ, and (c) the third harmonic η_3/λ for mode number $m = 3, 6$, and 30, respectively. The RTI growth is perturbed by both interface and velocity perturbations with $\alpha = v = 0.0005\lambda$ for $A = 1$. The planar results (dotted)[20] are plotted for comparison.

The mode number m dependence of the first three harmonics is displayed in Fig. 3. As can be seen in Fig. 3(a), the amplitude of the fundamental mode ($\eta_1 = \eta_{1,1} + \eta_{3,1}$) grows with increasing time γt, until reaching a maximum where the fundamental mode is saturated by the third-order negative feedback. The maximum amplitude is called the saturation amplitude. The amplitude of the fundamental mode is affected by the mode number m. The low-mode perturbation will lead to a larger maximum amplitude of η_1. For relatively small perturbations $\alpha = v = 0.0005\lambda$, the planar results[20] are recovered for $m = 30$. The evolution of the second harmonic ($\eta_2 = \eta_{2,2}$) is shown in Fig. 3(b), the phase of the second harmonic is shifted by π against the fundamental mode. Thus, the normalized amplitude η_2/λ is negative compared to the initial perturbations. The smaller mode number m leads to a larger absolute value of amplitude η_2. The η_2/λ is approximately identical to the planar result[20] for $m = 30$. The phase of the third harmonic ($\eta_3 = \eta_{3,3}$) is identical to the fundamental mode. The amplitude of the third harmonic η_3/λ in cylindrical geometry is larger than that in planar RTI for $A = 1$. With the increasing mode number m, the planar result is recovered for fixed γt, which is shown in Fig. 3(c).

The nonlinear saturation amplitude (NSA) of the fundamental mode is defined as the linear growth amplitude of perturbation at a time when the amplitude of the fundamental mode η_1 is reduced by 10% compared to its corresponding linear growth $\eta_{1,1}$, namely, $(\eta_{1,1} - \eta_1)/\eta_{1,1} = 1/10$. The Atwood number A dependence of the normalized NSA η_s/λ is shown in Fig. 4 for $\alpha = v = 0.005\lambda$. For fixed mode number m, the normalized NSAs decrease with increasing Atwood number A. For low-mode number and small Atwood number perturbation, the NSA of the cylindrical RTI is much larger than the classical NSA of $\sim 0.1\lambda$,[4,20,22] which is a typical threshold for nonlinear RTI growth. This means that the low-mode perturbation of RTI growth in ICF implosions is very severe and hard to control. The high-foot implosion experiments on National Ignition Facility (NIF) indicated that the low-mode perturbation at the inner interface still grows faster, resulting in the deformation of the hot-spot.[28] Thus, special attention should be paid to controlling the low-mode RTI growth in ICF ignition target design.

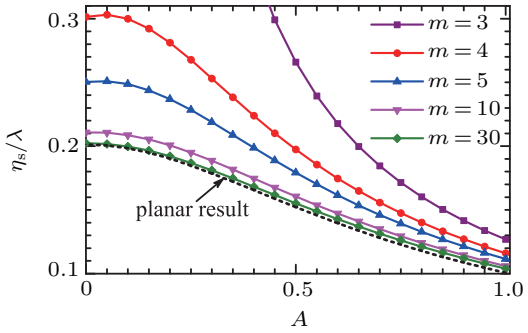


Fig. 4. (color online) The normalized NSAs η_s/λ versus the Atwood number A for $m = 3, 4, 5, 10$, and 30, respectively. The initial perturbation amplitudes are $\alpha = v = 0.0005\lambda$.

Figure 5 illustrates the initial perturbation dependence of the normalized NSAs for $m = 4$ and 10, respectively. The initial perturbation plays a more significant role in the NSA of the RTI by applying the interface perturbation alone than that by imposing the velocity perturbation alone, which can be seen in Figs. 5(a), 5(b), 5(d), and 5(e). When the RTI growth is initiated with only the velocity perturbation (Figs. 5(b) and 5(e)), the weak initial perturbation amplitude dependence of the NSA is displayed, whereas the Atwood number A still plays a pronounced role. When the RTI is initially perturbed with an interface perturbation, there exists a critical Atwood number A_c. When $A > A_c$, the NSA increases with increasing initial amplitude α, while the NSA decreases with increasing α for $A < A_c$. The A_c is ~ 0.4 and ~ 0.25, respectively, for mode number $m = 4$ and 10. That is to say, A_c decreases with increasing mode number m for the interface perturbation. This phenomenon can also be seen in Figs. 5(c) and 5(f), where $A_c \sim 0.3$ for $m = 4$ and $A_c \sim 0$ for $m = 10$ are obtained. It should be pointed out that the NSA of the fundamental mode initiated with interface perturbation $[\eta(0) = \alpha\cos(m\theta)]$ is approximately identical to that with velocity perturbation $[\dot{\eta}(0) = v\gamma\cos(m\theta)]$ for small perturbation amplitude $\alpha = v < 0.001\lambda$, which can also be seen in Fig. 1.

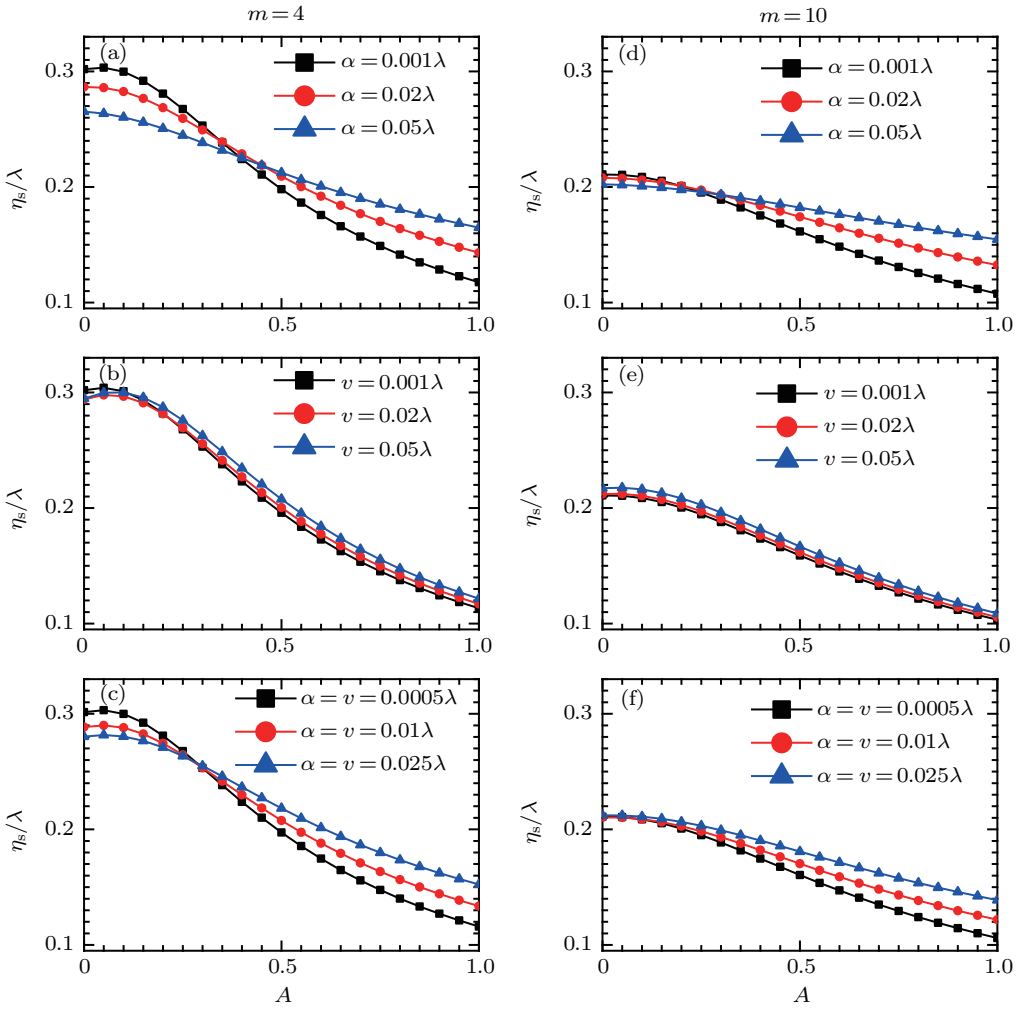


Fig. 5. (color online) The normalized NSAs versus the Atwood number for (a)–(c) $m = 4$ and (d)–(f) $m = 10$, respectively. The RTI growth is perturbed by only the interface perturbation [(a) and (d)], only the velocity perturbation [(b) and (e)], and both velocity and interface perturbations [(c) and (f)], respectively.

4. Conclusion

In this research, the WN growth of cylindrical RTI initiated with velocity and interface perturbations is studied analytically. There are coupling terms (containing αv, $\alpha^2 v$ and αv^2) between the velocity and interface perturbations in the WN region. When the initial interface perturbation amplitude is equal to the equivalent velocity amplitude, namely, $\alpha = v$, the difference between the WN growth of cylindrical RTI initiated by an interface perturbation alone and that by a velocity perturbation alone is negligibly small. The dependencies of the first three harmonics on the initial perturbation amplitudes are discussed in detail. The temporal evolutions of the first three harmonics are strongly dependent on the mode number. The low-mode perturbation will cause larger growth of the first three Fourier harmonics. The NSAs of the fundamental mode are greatly affected by the Atwood number A and mode number m. The smaller mode number m is, the larger the NSA of η_s will be. The normalized NSAs are influenced by the initial interface perturbation. When mode number m is large enough ($m \gg 30$) for small initial perturbation amplitude, the RTI growth in the planar case is recovered.[20,21] The present work is expected to enhance the understanding of the RTI evolution in cylindrical geometry and to be probably significant for the assessment of the RTI growth in ICF implosions.

Appendix A

The expressions of coefficients $a_1, \ldots, a_{10}$ and $b_1, \ldots, b_9$ are displayed as follows:

$$
\begin{aligned}
\xi_1 &= 8A^2m^2 + 8Am - 2m^2 + 1, \\
\xi_2 &= 24A^2m^2 + 32Am + 11, \\
\xi_3 &= A^2m^2 - Am + m^2, \\
\xi_4 &= 11A^2m^2 - 3Am - m^2 - 11, \\
\xi_5 &= 9A^2m^2 - Am + 3m^2 - 22, \\
a_1 &= 2\alpha^3\xi_1 + 2(5 + 6Am)v^2\alpha, \\
a_2 &= 2v^3\xi_1 + 2(5 + 6Am)\alpha^2 v, \\
a_3 &= 2(5 + 6Am)\left(v^3 + 2\alpha^2 v\right) + 6\alpha^2 v\xi_1, \\
a_4 &= 2(5 + 6Am)\left(\alpha^3 + 2v^2\alpha\right) + 6v^2\alpha\xi_1, \\
a_5 &= 8(2 + 3Am)v^2\alpha - (7 + 12Am - \xi_2)\,\alpha^3,
\end{aligned}
\tag{A1}
$$

$$
\begin{aligned}
a_6 &= 4(1+3Am)v^3+(5+\xi_2)\,v\alpha^2,\\
a_7 &= 3\sqrt{2}v^3+\sqrt{2}\,(6Am+\xi_2)\,v\alpha^2,\\
a_8 &= 3\sqrt{2}(1+2Am)\alpha^3+\sqrt{2}v^2\alpha\xi_2,\\
a_9 &= \left(1-4Am+6m^2+\xi_1\right)\alpha^3+6(1+2Am)v^2\alpha,\\
a_{10} &= \sqrt{3}\left(3+4Am+6m^2+\xi_1\right)\alpha^2 v, \qquad \text{(A2)}\\
b_1 &= -(2Am+5)v^2\alpha+\left(4A^2m^2-1\right)\alpha^3,\\
b_2 &= 2\left(\xi_3-2-m^2\right)v^3-2\left(A^2m^2-2m^2+8\right)\alpha^2 v,\\
b_3 &= (2Am-5+\xi_3)\,v^3+\xi_4\alpha^2 v,\\
b_4 &= \left(2A^2m^2+8-\xi_3\right)\alpha^3-\xi_5 v^2\alpha,\\
b_5 &= (2Am-1)v^3-\left(4m^2+5-4\xi_3\right)\alpha^2 v,\\
b_6 &= \sqrt{2}v^3-\sqrt{2}\left(4A^2m^2-3\right)v\alpha^2,\\
b_7 &= \sqrt{2}(2Am+1)\left(\alpha^3-2Amv^2\alpha\right)+3\sqrt{2}v^2\alpha,\\
b_8 &= \xi_3\left(v^3-\alpha^2 v\right)-2v^3,\\
b_9 &= -\xi_3\left(\alpha^3-v^2\alpha\right)-2v^2\alpha. \qquad \text{(A3)}
\end{aligned}
$$

Acknowledgment

The author (Hong-Yu Guo) thanks Prof. Xian-Tu He for his useful discussion and help.

References

[1] Rayleigh L 1883 *Proc. London Math. Soc.* **14** 170
[2] Taylor G 1950 *Proc. R. Soc. Lond. A* **201** 192
[3] Zhang Y and Ding N 2008 *Chin. Phys. B* **17** 2994
[4] Lindl J D, Amendt P, Berger R L, Glendinning S G, Glenzer S H, Haan S W, Kauffman R L, Landen O L and Suter L J 2004 *Phys. Plasmas* **11** 339
[5] Wang L F, Ye W H, He X T, Wu J F, Fan Z F, Xue C, Guo H Y, Miao W Y, Yuan Y T, Dong J Q, Jia G, Zhang J, Li Y J, Liu J, Wang M, Ding Y K and Zhang W Y 2017 *Sci. China Phys. Mech. Astron.* **60** 055201
[6] Hsing WW, Barnes C W, Beck J B, Hoffman N M, Galmiche D, Richard A, Edwards J, Graham P, Rothman S and Thomas B 1997 *Phys. Plasmas* **4** 1832
[7] Guo H Y, Yu X J, Wang L F, Ye W H, Wu J F and Li Y J 2014 *Chin. Phys. Lett* **31** 044702
[8] Wang L F, Wu J F, Guo H Y, Ye W H, Liu J, Zhang W Y and He X T 2015 *Phys. Plasmas* **22** 082702
[9] Mikaelian K O 1982 *Phys. Rev. A* **26** 2140
[10] Guo H Y, Wang L F, Ye W H, Wu J F and Zhang W Y 2017 *Chin. Phys. Lett.* **34** 075201
[11] Yang B L, Wang L F, Ye W H and Xue C 2011 *Phys. Plasmas* **18** 072111
[12] Ye W H, Zhang W Y and He X T 2002 *Phys. Rev. E* **65** 057401
[13] Wang L F, Ye W H, He X T, Zhang W Y, Sheng Z M and Yu M Y 2012 *Phys. Plasmas* **19** 100701
[14] Yan R, Betti R, Sanz J, Aluie H, Liu B and Frank A 2016 *Phys. Plasmas* **23** 022701
[15] Jacobs J W and Catton I 1988 *J. Fluid Mech.* **187** 329
[16] Guo H Y, Wang L F, Ye W H, Wu J F and Zhang W Y 2017 *Chin. Phys. Lett* **34** 045201
[17] Haan S W 1991 *Phys. Fluids B* **3** 2349
[18] Garnier J and Masse L 2005 *Phys. Plasmas* **12** 062707
[19] Wang L F, Guo H Y, Wu J F, Ye W H, Liu J, Zhang W Y and He X T 2014 *Phys. Plasmas* **21** 122710
[20] Wang L F, Ye W H and Li Y J 2010 *Chin. Phys. Lett.* **27** 025203
[21] Wang L F, Wu J F, Fan Z F, Ye W H, He X T, Zhang W Y, Dai Z S, Gu J F and Xue C 2012 *Phys. Plasmas* **19** 112706
[22] Liu W H, Wang L F, Ye W H and He X T 2012 *Phys. Plasmas* **19** 042705
[23] Ryutov D D, Cuneo M E, Herrmann M C, Sinars D B and Slutz S A 2012 *Phys. Plasmas* **19** 062706
[24] Betti R, Lobatchev V and McCrory R L 1998 *Phys. Rev. Lett.* **81** 5560
[25] Goncharov V N 1999 *Phys. Rev. Lett.* **82** 2091
[26] Amendt P, Colvin J D, Ramshaw J D, Robey H F and Landen O L 2003 *Phys. Plasmas* **10** 820
[27] Wang L F, Wu J F, Ye W H, Zhang W Y and He X T 2013 *Phys. Plasmas* **20** 042708
[28] Dittrich T R, Hurricane O A, Callahan D A, Dewald E L, Doppner T, Hinkel D E, Berzak Hopkins L F, LePape S, Ma T, Milovich J, Moreno J C, Patel P K, Park H S, Remington B A and Salmonson J 2014 *Phys. Rev. Lett.* **112** 055002